Kinetic energy spectra and angular distributions of projectile-like fragments in $^{12,13}C + ^{93}Nb$ reactions

T. N. Nag,[1,3] R. Tripathi,[1,3,*] S. Sodaye,[1,3] K. Sudarshan,[1,3] S. Santra,[2,3] K. Ramachandran,[2] A. Kundu,[2,3] D. Chattopadhyay,[2,3] A. Pal,[2] and P. K. Pujari[1,3]

[1]*Radiochemistry Division, Bhabha Atomic Research Centre, Mumbai - 400085, India*

[2]*Nuclear Physics Division, Bhabha Atomic Research Centre, Mumbai - 400085, India*

[3]*Homi Bhabha National Institute, Anushaktinagar, Mumbai-400094, India*

(Received 20 September 2019; revised 11 June 2020; accepted 15 July 2020; published 10 August 2020)

Kinetic-energy spectra and angular distributions of the projectile-like fragments were measured in $^{12,13}C + ^{93}Nb$ reactions at $E_{lab} = 65$ MeV to investigate the reaction mechanisms involving the role of projectile and target structures. It has been observed that one-nucleon pick-up reactions lead to the formation of target-like fragments predominantly in the ground state, whereas nucleon transfer to the target occurs predominantly in the excited states for both $^{12}C + ^{93}Nb$ and $^{13}C + ^{93}Nb$ reactions. In the case of $^{93}Nb(^{12}C, ^{15}N)^{90}Zr$ reactions, a significant yield was observed for ^{15}N ("$1p + 2n$" pick-up) indicating the role of the $N = 50$ shell in ^{90}Zr. Observation of a systematic increase in the forward peaking of the angular distributions of projectile-like fragments with an increasing number of nucleon transfers indicates an increase in the projectile-target overlap with increasing mass transfer. Angular distributions for inelastic scattering as well as transfer channels populating various states of projectile-like fragments and/or target-like fragments were calculated simultaneously by using the coupled reaction channels code FRESCO and were in reasonable agreement with the experimental data. New (modified) spectroscopic amplitudes have been proposed for some of the unknown (known) overlapping states for calculating transfer cross sections. In the case of $^{13}C + ^{93}Nb$, the transfer channels corresponding to "$2n$" and "$1p + 1n$" pick-up channels were not observed. This may be due to the higher N/Z ratio of the projectile, highlighting the importance of projectile structure in addition to that of the target.

DOI: 10.1103/PhysRevC.102.024610

I. INTRODUCTION

Nuclear reactions involving the exchange of a few nucleons between target and projectile have been extensively studied for the last few decades to investigate the mechanisms involved [1–10]. The heavy-ion-induced nuclear reactions depend on various entrance channel parameters such as incident projectile energy [11,12], angular momentum [13–16], and mass asymmetry [17–19]. Apart from these parameters, projectile structure [20,21] also plays an important role in governing the stripping or pick-up reactions involving the exchange of nucleons between target and projectile. In the collision of projectile and target nuclei, apart from the complete fusion, there are possibilities of many other nucleon-exchange mechanisms, such as quasi-elastic transfer (QET), deep inelastic collisions, and incomplete fusion (ICF) reactions [4,22]. Incomplete fusion reactions involve significant overlap of the projectile and target nuclei, leading to large mass transfer. Measurements of cross sections of projectile-like fragments (PLFs) in $^{19}F + ^{66}Zn$ [7] and $^{19}F + ^{89}Y$ [6] reactions clearly show a distinct behavior of reaction channels involving different amount of mass transfer with the variation of beam energy. In these studies, it was observed that the cross sections of lighter PLFs formed in large mass transfer channels fall more rapidly with decreasing beam energy compared with those of heavier PLFs formed in small mass transfer channels. This observation was attributed to the requirement of a significant overlap of the projectile and target nuclei in ICF reactions. Such collision trajectories would lead to complete fusion at lower beam energy, resulting in rapid fall of ICF cross section. Sodaye *et al.* [12] measured kinetic energy and angular distributions of PLFs in $^{12}C + ^{169}Tm$ at 7 MeV/nucleon beam energy for different reaction channels. Similar measurements were carried out by Kumar *et al.* [23] for the $^{19}F + ^{159}Tb$ reaction system. Complimentary to these studies, evaporation residue cross sections were measured in various reaction systems, such as $^{12,13}C + ^{181}Ta$ [24], $^{12}C + ^{93}Nb$, and $^{16}O + ^{89}Y$ [25] to investigate the role of projectile structure in ICF reactions. Enhancement in the probability of some specific channels due to cluster structures of the projectiles have also been investigated in other systems [11,26].

Various models were proposed to explain observables of incomplete mass transfer reactions, including massive transfer or ICF reactions. According to the break-up fusion model of Udgawa and Tamura [27], ICF involves fragmentation of the projectile under the influence of the target nucleus followed by the capture of one of the fragments produced. Zagraebav

*rahult@barc.gov.in

et al. [28] used multistep direct reaction theory to explain QET and massive transfer reactions. According to the overlap model, the overlapping volume between projectile and target nuclei governs the amount of mass exchanged [29–31]. The model proposed by Morgenstern *et al.* [17] relates ICF cross sections to entrance channel mass asymmetry. The sum-rule model provides an approach to explain the cross sections of PLFs formed in stripping or pick-up of a few nucleons as well as massive transfer reactions. According to this model, the onset of ICF is related to the vanishing of pockets in the entrance channel potential for complete fusion at critical angular momentum $l_{\rm crit}$, so that higher-l waves predominantly lead to reactions involving incomplete mass transfer for which pockets in the entrance channel potential reappear [32]. All these theoretical models hold good at higher beam energies, which is more than about ≈10 MeV/u. However, at lower beam energies, the reactions involving incomplete mass transfer are dominated by stripping or pick-up of only a few nucleons. The formation of PLFs with masses close to that of the projectile in QET reactions can be described more appropriately by direct reaction models, for example, the coupled reaction channels code FRESCO [33].

At lower beam energies, i.e., energies not too much above the entrance channel Coulomb barrier, structures of the projectile and the target can play important roles in governing the cross sections for different stripping and pick-up reaction channels. Study of such reactions is important due to their intimate connection to the reactions involving radioactive nuclei away from the beta stability line. For example, studies carried out with ^{6}He, revealed its di-neutron structure with a ^{4}He core along with two valence neutrons [34–36]. Similarly, in studies involving ^{16,18}O + ^{174}Yb reactions, Sahu *et al.* observed strongly correlated "2n" transfer in ^{18}O-induced reactions, indicating an ^{16}O(core)+2n(valence) structure [37]. Similar results were observed in ^{16,18}O + ^{164}Dy, ^{208}Pb reactions [38]. These structures arise due to the presence of nucleons outside the magic number configuration. In the studies by Sahu *et al.* for ^{11}B + ^{208}Pb, ^{209}Bi reactions, an enhancement of proton pick-up was observed in the ^{11}B + ^{209}Bi reaction, indicating the role of the closed-shell configuration of target-like fragment (TLF) ^{208}Pb [39]. It would be important to carry out such studies with other nuclei with a greater number of nucleons outside the magic number configuration. In the study of reactions ^{7}Li + ^{89}Y [40] and ^{7}Li + ^{93}Nb [41], the neutron stripping cross section was obtained by correlated measurement of ^{4}He + d arising from the break-up of PLF ^{6}Li. In these studies, some difference in the cross sections for the two reactions was observed for the low-excitation-energy range of ^{6}Li; however, the difference was not noticeable when the whole excitation-energy range was considered. In these studies, no results have been given for neutron pick-up channels. These studies indicate that the observation of the effect of shell closure may be projectile dependent. Also, it would be important to measure the yields of the PLFs formed in neutron pick-up channels to get conclusive information about the effect of shell closure on the transfer process.

In the present work, kinetic-energy spectra, angular distributions, and cross sections of the projectile-like fragments have been measured in ^{12,13}C + ^{93}Nb reactions at the beam energy of 65 MeV to investigate the formation mechanism of different PLFs and states involved in different stripping or pick-up channels. The ^{93}Nb nucleus has one proton and two neutrons out of its closed-shell semi-magic configuration with 50 neutrons. So, a transfer reaction involving pickup of either one proton or two neutrons or both by a projectile from a ^{93}Nb target can lead to a more stable structure of the residual target in the exit channel. Thus, the target structure is expected to play an important role in governing the cross sections for different transfer channels. In addition, cross sections for these transfer channels would also depend on the projectile structure. To investigate the effect of the N/Z ratio of the projectile, two projectiles ^{12}C and ^{13}C have been chosen. Using the coupled reaction channels code FRESCO, calculations have been performed to obtain the angular distributions for inelastic excitations and nucleon stripping or pick-up channels, which have been compared with the experimental data.

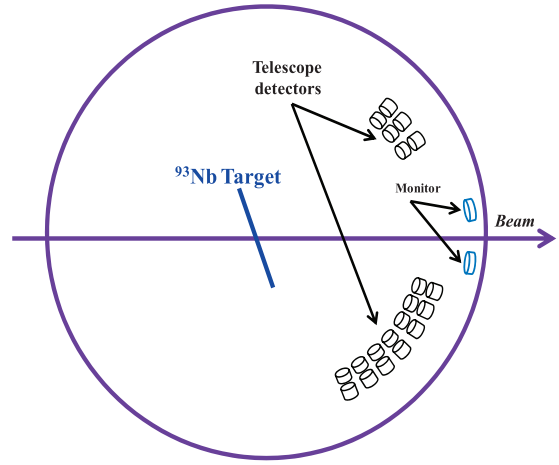

FIG. 1. Schematic diagram of detector setup inside a general purpose scattering chamber.

II. EXPERIMENTAL DETAILS

Experiments were carried out at BARC-TIFR Pelletron-LINAC facility at Tata Institute of Fundamental Research, Mumbai, India. A self-supporting target of ^{93}Nb of thickness ≈400 μg/cm^2 was bombarded with 65 MeV ^{12,13}C beams in a scattering chamber with a diameter of 1.5 m. Ten silicon-detector-based ΔE-E telescopes were used to detect the outgoing PLFs formed in various transfer channels in order to obtain the angular distributions. Two monitor detectors were placed at ±20° to detect the elastically scattered beam particles to normalize for the variation in the incident flux. Figure 1 shows a schematic diagram of the detector setup in the scattering chamber. The thickness of the ΔE and E detectors were in the range of 25–50 μm and 300–1000 μm, respectively. The angular distributions of PLFs were measured in the angular range of 20°−70°. Data were acquired by using a VME-based multiparameter data-acquisition system.

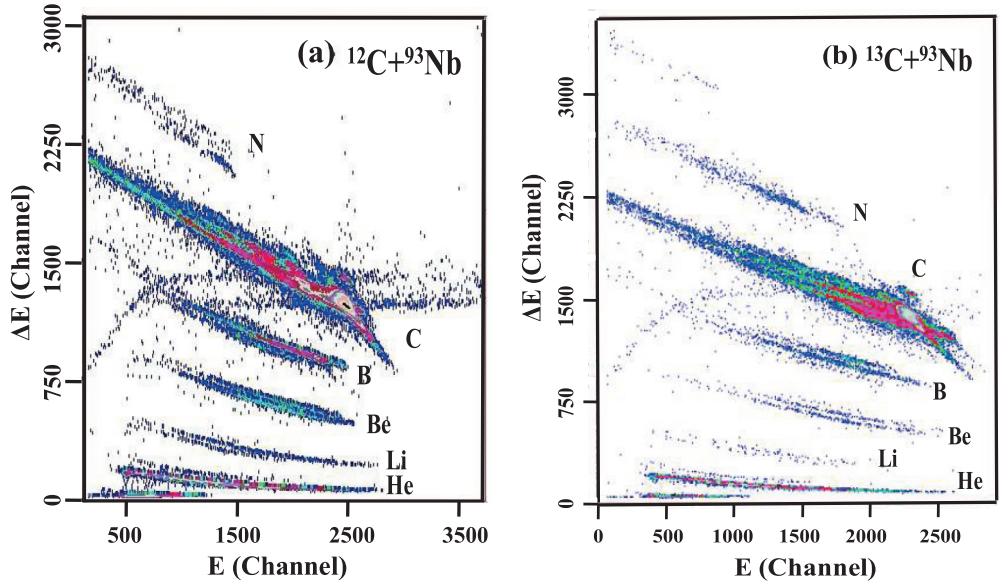

FIG. 2. Typical two-dimensional (ΔE versus E) raw spectra showing the PLFs formed in (a) $^{12}C + ^{93}Nb$ and (b) $^{13}C + ^{93}Nb$ reactions at $E_{lab} = 65$ MeV.

III. RESULTS AND DISCUSSIONS

A. Kinetic-energy spectra of projectile-like fragments

Figure 2 shows a typical two-dimensional (ΔE versus E) spectrum of the PLFs formed in $^{12,13}C + ^{93}Nb$ reactions at 65 MeV beam energy. The particle identifier (PI) spectrum was generated after relative gain matching of the E and ΔE detectors [42]. A y-axis projection of the particle identifier spectrum is shown in Fig. 3, where peaks due to PLFs formed in different stripping and pick-up channels in $^{12,13}C + ^{93}Nb$ reactions are marked. In both the reaction systems, PI spectra for "carbon isotopes" are not shown due to the large background from the tail of the elastic peak. It is important to note an unusual trend in the yields of nitrogen isotopes formed in the $^{12}C + ^{93}Nb$ reaction. Although the yield decreases from ^{13}N to ^{14}N, it again increases for ^{15}N, which is formed along with ^{90}Zr having the closed-shell configuration with 50 neutrons. This observation suggests that the closed-shell structure of ^{90}Zr with 50 neutrons possibly favors the formation of ^{15}N. A significant yield was also observed for the two-neutron pick-up channel in the $^{12}C + ^{93}Nb$ reaction system, which leads to the formation of ^{14}C as PLF and ^{91}Nb as TLF with the closed-shell configuration of 50 neutrons, although not shown in the PI spectra as discussed earlier. In the case of carbon, the kinetic-energy spectra were obtained by selecting carbon isotopes other than the beam.

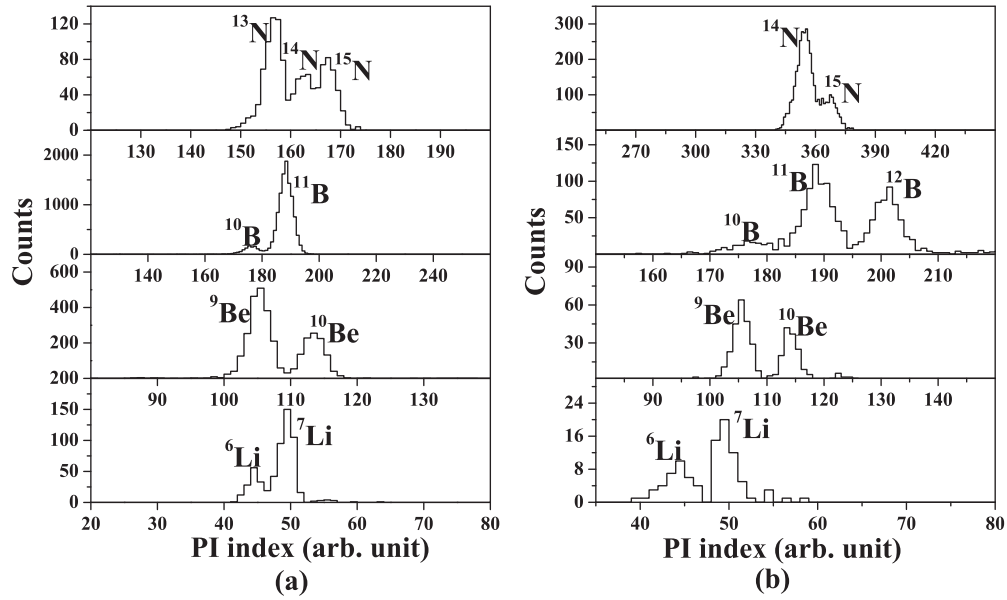

FIG. 3. PI index spectra of PLFs formed in (a) $^{12}C + ^{93}Nb$ and (b) $^{13}C + ^{93}Nb$ at $E_{lab} = 65$ MeV.

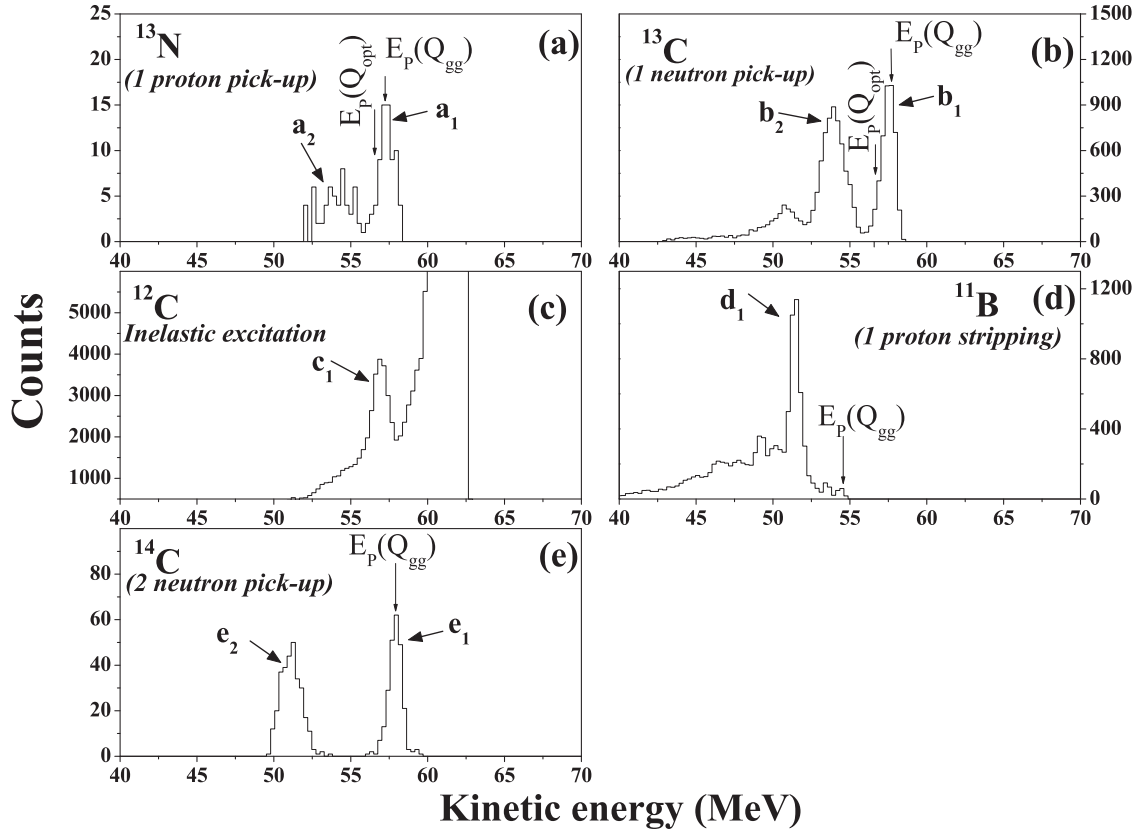

FIG. 4. Kinetic-energy spectra of PLFs (a) ^{13}N, (b) ^{13}C, (c) ^{12}C, (d) ^{11}B, and (e) ^{14}C formed in $^{12}C + ^{93}Nb$ reaction at $E_{lab} = 65$ MeV and $\theta_{lab} = 37.5^\circ$. The arrow captioned with $E_P(Q_{gg})$ represents the kinetic energy of the PLFs obtained from kinematic equations using Q_{gg} values and arrow captioned with $E_P(Q_{opt})$ represents the kinetic energy of the PLFs obtained using the prescription of Mermaz [43]. The identified energy states of PLFs and TLFs involved in various stripping and pick-up mechanisms are mentioned in the figure as [a_1 : ^{13}N(g.s., $1/2^-$), ^{92}Zr(g.s., 0^+)], [a_2 : ^{13}N(2.635 MeV, $^1/_2{}^+$), ^{92}Zr(g.s., 0^+)], [b_1 : ^{13}C(g.s., $1/2^-$), TLF*], [b_2 : ^{13}C(3.68 MeV, $3/2^-$), TLF*], [c_1 : ^{12}C(4.44 MeV, 2^+), ^{93}Nb(g.s., $9/2^+$)], [d_1 : ^{11}B(2.124 MeV, $1/2^-$), ^{94}Mo (0.871 MeV, 2^+)], [e_1 : ^{14}C(g.s., 0^+), ^{91}Nb(g.s., $9/2^+$)], [e_2 : ^{14}C(6.589 MeV, 0^+), ^{91}Nb(g.s., $9/2^+$)] (*: population of multiple excited states of TLF in the energy range up to 500 keV).

Figures 4 and 5 show the kinetic-energy spectra for different PLFs formed in $^{12}C + ^{93}Nb$ and $^{13}C + ^{93}Nb$ reactions, respectively. The kinetic energies of the PLFs corresponding to Q_{gg} and Q_{opt} values for different stripping and pick-up channels are marked by the arrows in each figure. The Q_{opt} values for various channels were calculated by using the prescription of Mermaz [43]. However, for some of the PLFs, for example, ^{11}B in the $^{12}C + ^{93}Nb$ reaction, calculated Q_{opt} values were lower than the Q_{gg} values and are, therefore, not shown for those PLFs. This situation arises because the assumption that the outgoing PLF goes with the beam velocity is not valid at lower beam energies for reaction channels with highly negative Q_{gg} values. This is the case for ^{11}B in the $^{12}C + ^{93}Nb$ reaction for which Q_{gg} is -7.47 MeV, and for ^{12}B in $^{13}C + ^{93}Nb$ for which Q_{gg} is -9.043 MeV. It can be seen from Figs. 4 and 5 that the most intense peaks in the kinetic-energy spectra of different PLFs are not strongly correlated to the Q_{opt} values, indicating the dominant role played by the discrete states involved in the stripping and pick-up channels. In the kinetic-energy spectra of the projectile and PLFs, different excited states of the projectile, PLFs and target-like fragments (TLFs) involved in inelastic excitation and in various stripping and pick-up channels were identified. As seen from Fig. 4(a), in the $^{12}C + ^{93}Nb$ reaction, the proton pick-up channel resulted in the formation of the PLF ^{13}N and the TLF ^{92}Zr predominantly in their ground states. In contrast, one-proton stripping resulted in the formation of both the PLF ^{11}B (2.124 MeV, $1/2^-$) and the TLF ^{94}Mo (0.871 MeV, 2^+) in their first-excited states, as seen from Fig. 4(d). This observation indicates that the proton-stripping mechanism proceeds through the excitation of the proton pair present in the $1p_{3/2}$ level in ^{12}C followed by pair breaking. As seen from Fig. 4(b), the one-neutron pick-up channel leads to the formation of ^{13}C in the ground state ($1/2^-$) and the 3.68 MeV, $3/2^-$ excited state with comparable intensities along with the population of multiple excitations of closely spaced energy levels (up to $\approx$500 keV) of TLF ^{92}Nb. The inelastic scattering of ^{12}C predominantly leads to the population of the 4.44 MeV, 2^+ excited state of ^{12}C, as shown in Fig. 4(c). The kinetic-energy spectra of ^{14}C formed in two-neutron pick-up is shown in Fig. 4(e). It can be seen from this figure that two-neutron pick-up leads to the formation of ^{14}C in its ground state (0^+) and in the 6.589 MeV, 0^+ excited state along with the formation of ^{91}Nb in its ground state ($9/2^+$). In the

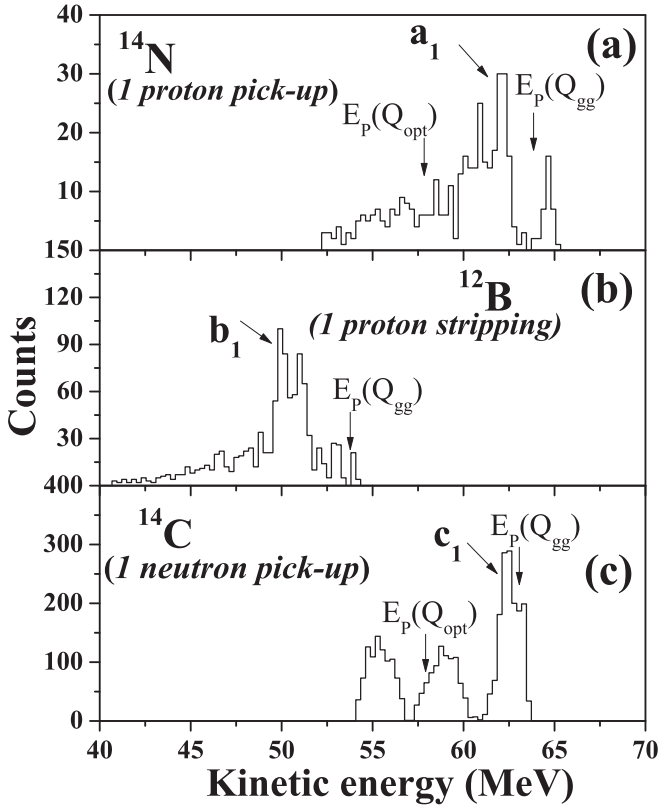

FIG. 5. Kinetic-energy spectra of PLFs (a) ^{14}N, (b) ^{12}B, and (c) ^{14}C formed in ^{13}C + ^{93}Nb reaction obtained at $\theta_{lab} = 30^\circ$ for $E_{lab} = 65$ MeV. The arrow captioned with $E_P(Q_{gg})$ represents the kinetic energy of the PLFs obtained from kinematic equations with Q_{gg} values, and arrow captioned with $E_P(Q_{opt})$ represents the kinetic energy of the PLFs obtained using the prescription of Mermaz [43]. The identified energy states of PLFs and TLFs involved in various stripping and pick-up mechanisms are mentioned in the figure as [a$_1$: ^{14}N(2.31 MeV, 0$^+$), ^{92}Zr(g.s., 0$^+$)], [b$_1$: ^{12}B(2.62 MeV, 1$^-$), ^{94}Mo 1.573 MeV 4$^+$], [c$_1$: ^{14}C(g.s., 0$^+$), TLF*] (*: population of multiple excited states of TLF in the energy range up to 500 keV).

^{13}C + ^{93}Nb reaction, the one-proton pick-up channel leads to the formation of ^{14}N predominantly in the first-excited state (2.31 MeV, 0$^+$) along with ^{92}Zr in the ground state (0$^+$), as shown in Fig. 5(a). In the one-proton stripping channel forming ^{12}B and ^{94}Mo, both PLF and TLF are predominantly formed in their excited states, as shown in Fig. 5(b). Figure 5(c) shows the kinetic-energy spectrum of ^{14}C formed in a one-neutron pick-up reaction. The highest-energy peak in this spectrum corresponds to the formation of ^{14}C in the ground state (0$^+$) along with the population of multiple closely spaced energy levels (up to ≈500 keV) of the TLF ^{92}Nb. The other two peaks at lower energies have contributions from multiple excited states of PLFs and TLFs.

B. Angular distributions of projectile-like fragments

The elastic-scattering angular distributions for ^{12,13}C + ^{93}Nb reactions at 65 MeV beam energy are shown in Fig. 6. The elastic-scattering data were fit by using the coupled reaction channels code FRESCO [33]. The potential parameters obtained from the fit are given in Table I. The fitting of elastic-scattering data gave the grazing angle values as 50.3° and 47.6° for the ^{12}C + ^{93}Nb and ^{13}C + ^{93}Nb reactions, respectively. The elastic scattering data points at the forward angles in the flat region were normalized to unity and the normalization factor was subsequently used for scaling the angular distributions of PLFs. From the ΔE-E spectra at different angles, the lab angular distributions were obtained and were transformed into the center-of-mass (c.m.) frame of reference by using standard kinematic equations with average kinetic energies obtained from kinetic-energy spectra of PLFs in the c.m. frame of reference [44]. The c.m. angular distributions of the PLFs with $Z = 3-7$ are shown in Fig. 7(a) for ^{12}C + ^{93}Nb reaction and in Figs. 7(b) and 7(c) for the ^{13}C + ^{93}Nb reaction. The uncertainties in the experimental data points are due to the statistics. Angular distributions for PLFs with $Z \leqslant 2$ have not been included due to the significant contribution from the compound nucleus emission. In addition, break-up of ^{8}Be would also contribute to the formation of alpha particles. Also, the angular distribution of ^{14}C formed in ^{12}C + ^{93}Nb reaction is not shown here because its formation involved only discrete energy states of PLFs and TLFs and, therefore, is shown later as a part of Fig. 8, which shows angular distributions for transfer and pick-up involving discrete states. As seen from Fig. 7, angular distributions of

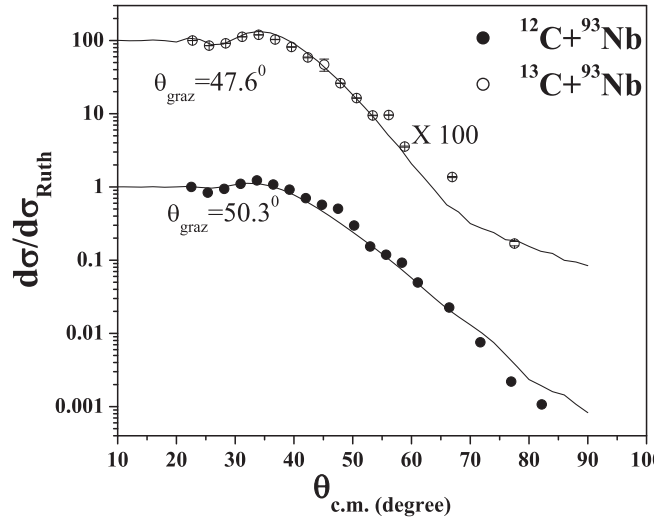

FIG. 6. Plot of elastic-scattering data for ^{12,13}C + ^{93}Nb system at $E_{lab} = 65$ MeV. Solid lines are obtained by reproducing the elastic-scattering data using the code FRESCO [33]. Grazing angles in center-of-mass frame of reference are given in the figure.

TABLE I. Optical model potential parameters obtained by reproducing the elastic-scattering data using the code FRESCO [33].

	V_0 (MeV)	R_0 (fm)	a_0 (fm)	W_S (MeV)	R_W (fm)	a_W (fm)
^{12}C + ^{93}Nb	77.9	1.194	0.538	35.57	1.211	0.652
^{13}C + ^{93}Nb	81.8	1.180	0.596	35.36	1.125	0.596

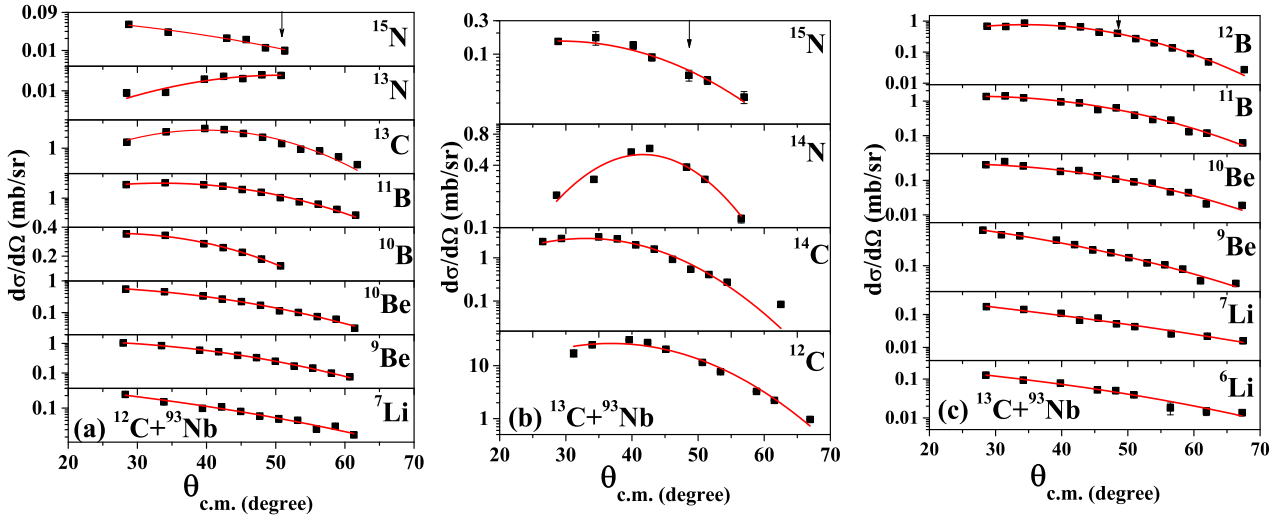

FIG. 7. Center of mass angular distributions of the PLFs for $Z = 3-7$ formed in (a) $^{12}C + ^{93}Nb$ and (b), (c) $^{13}C + ^{93}Nb$ reactions at $E_{lab} = 65$ MeV. Solid lines were obtained from Gaussian fitting. The arrow marks the grazing angle.

the PLFs formed through the exchange of a few nucleons in both $^{12}C + ^{93}Nb$ and $^{13}C + ^{93}Nb$ reactions peak close to the respective grazing angles, which are marked by arrow. This observation indicates that PLFs with mass closer to the projectile (involving small mass transfer) are predominantly formed in the peripheral collisions between projectile and target through a quasi-elastic transfer process similar to that observed in earlier studies [6,7,23]. Observation of an increase in the forward peaking of the angular distributions of the PLFs with their decreasing mass indicates a significant contribution from the nuclear interaction of the participating nuclei. This is consistent with the requirement of significant overlap of the projectile and the target nuclei in incomplete fusion or massive transfer reactions. The strongly-forward-peaked angular distribution of ^{15}N can also be explained in the same way because its formation also requires significant mass transfer, although in the opposite direction.

Angular distributions for inelastic scattering and of PLFs close to the projectile, involving various states of PLFs and TLFs, were also obtained and are shown in Figs. 8(a)–8(f). The peak positions of angular distributions corresponding to these states do not differ significantly as compared with the overall angular distributions of respective PLFs, indicating that the average impact parameters for collision trajectories corresponding to different transfer channels are correlated more with the mass transfer than with the energy dissipation. Angular distributions for these channels were also calculated by using the coupled reaction channels code FRESCO for direct reactions [33]. The potential parameters obtained from the fitting of elastic scattering data were supplied as input. Binding energies and spectroscopic factors used in the present calculations are given in Table II. The potential parameters for the interaction of transferred nucleons with the core are obtained in the code by reproducing the respective binding energies. The quantum states of the transferred nucleon in the composite are given in the table and were supplied as input to the FRESCO calculations. Wherever available, spectroscopic factors were taken from the literature [45–50]. When more than one value was available in the literature, the value that gave best agreement with the experimental data was chosen. However, some of the literature values had to be modified to reproduce the corresponding experimental peak cross sections. For some of the channels, information on the spectroscopic factor was not available. For such cases, new spectroscopic factors were obtained from the present study by reproducing the peak cross sections which are given in the Table II. The calculated angular distributions are shown as dotted lines in Figs. 8(a)–8(f). The angular distribution for the inelastic state of ^{12}C (4.44 MeV, 2^+) is shown in Fig. 8(a). The large error bars in the experimental data are due to the background of the elastic tail, which increased the error on extracted peak areas. Angular distributions for the population of discrete states of PLFs (^{13}C) and TLFs (^{92}Nb) in one-neutron pick-up in the $^{12}C + ^{93}Nb$ reaction is shown in Fig. 8(b). FRESCO calculation for this channel includes the coupling of close-by energy levels of ^{92}Nb up to 500 keV because these energy levels would be mixed into the peak observed in the kinetic-energy spectra. To include the contribution from negative-parity states of ^{92}Nb in the neutron pick-up channel, coupling of inner negative-parity states ($1f_{5/2}$, $2p_{3/2}$) of ^{93}Nb have been considered in the calculation, which is given in Table II. Theoretical calculations for two-neutron pick-up channels forming ^{91}Nb in the ground state ($9/2^+$) and ^{14}C in the ground state (0^+) as well as in the 6.589 MeV, 0^+ state is shown in Fig. 8(c). In the calculation for this channel, both sequential ($^{12}C + n \rightarrow {}^{13}C$; $^{13}C + n \rightarrow {}^{14}C$) and simultaneous pick-up ($^{12}C + 2n \rightarrow {}^{14}C$) of two neutrons leading to the formation of ^{14}C along with ^{91}Nb were considered. As observed from Fig. 8(c), the angular distribution of ^{14}C (ground state, 0^+) could be explained reasonably by FRESCO calculations; however, a large deviation was observed for the angular distribution of ^{14}C in the excited state (6.589 MeV, 0^+). Figures 8(d) and 8(e) show the PLF angular distribution for one-proton pick-up and stripping channels, respectively, in the $^{12}C + ^{93}Nb$ reaction. A significantly large spectroscopic factor was required for $^{12}C(\text{g.s.}, 0^+) \rightarrow {}^{11}B(2.124\,\text{MeV}, 1/2^-)$ in

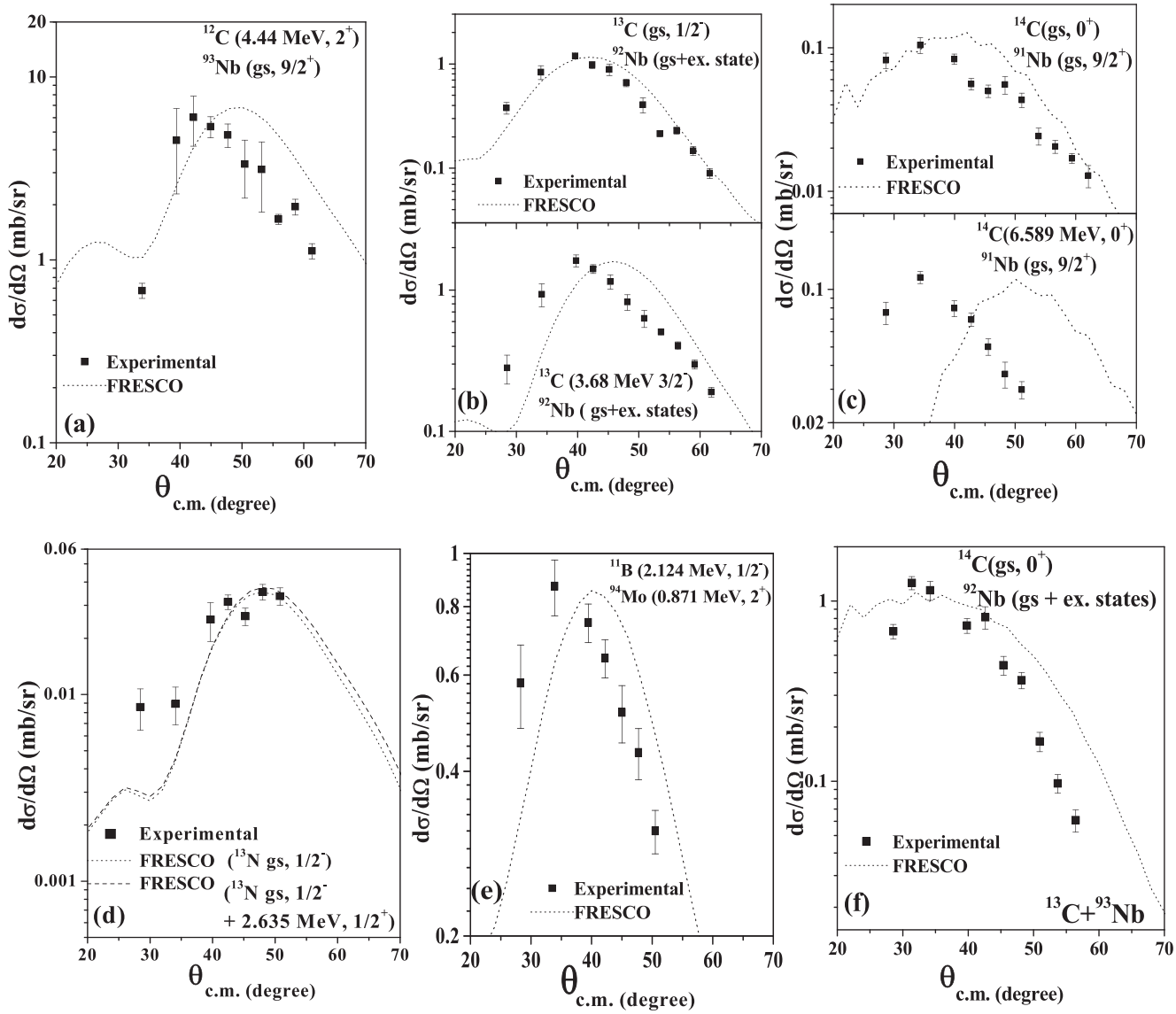

FIG. 8. Plots of angular distribution of specific states of the PLFs and TLF populated in different transfer reactions or inelastic excitation which were formed in (a)–(e) ^{12}C + ^{93}Nb and (f) ^{13}C + ^{93}Nb reactions. Dotted lines are FRESCO [33] calculations.

the one-proton stripping channel. The comparison of experimental and calculated angular distributions corresponding to the population of specific states of ^{14}C and ^{92}Nb formed in the one-neutron pick-up channel in ^{13}C + ^{93}Nb reaction has been shown in Fig. 8(f). As seen from these comparisons, the calculations reasonably describe the experimental angular distributions, with a general observation that experimental angular distributions are more forward peaked with respect to the calculation with varying magnitude. It was possible to get better agreement by varying the potential parameters for specific channels; however, it led to a significant mismatch in the elastic channel. This possibly indicates an inadequacy of the parameter sets obtained from elastic scattering in explaining certain channels showing significant deviation.

To determine the formation cross sections of the PLFs, the plots of differential cross sections $(d\sigma/d\Omega)$, multiplied with $2\pi \sin\theta_{\text{c.m.}}$, were fit to a Gaussian function. The approximation of Gaussian fitting has been adopted for the comparison of cross-section data for the two reaction systems and its correlation to Q_{gg} values for different transfer channels. The partial angular coverage in experimental measurements and deviation from the Gaussian function will be accounted for, to some extent, as enhanced uncertainty on the extracted cross sections. The fitted Gaussian curves (shown as solid lines in Fig. 7) for different PLFs were integrated to obtain their formation cross sections. The comparison of cross sections of PLFs formed in ^{12}C- and ^{13}C-induced reactions are shown in Fig. 9. The dark gray part of the bars represent the cross sections of the PLFs corresponding to the angular range covered in the experiment, and the light gray part of the bars represent the cross sections obtained from the extrapolation of the fitted curve up to 0° and 180°. The uncertainties, which are shown in the figure, are due to the fitting. It should be mentioned here that the cross section data for

TABLE II. Structure information and spectroscopic factors S for the overlaps $A = C \pm x$ corresponding to different states of nuclei A, C, and x used in the FRESCO calculations. "BE" is the binding energy of the nucleon.

A	C	x	n, l, j	BE (MeV)	S (this work)	S (reported value)	Ref.
^{12}C(g.s., 0^+)	^{11}B(g.s., $3/2^-$)	$-p$	$1p_{3/2}$	15.957	4.1	1.85–4.1	[45]
^{12}C(g.s., 0^+)	^{11}B(2.124 MeV, $1/2^-$)	$-p$	$1p_{1/2}$	18.081	13.69	[a]	
^{93}Nb(g.s., $9/2^+$)	^{94}Mo(g.s., 2^+)	$+p$	$1g_{9/2}$	8.490	1.0	[a]	
^{93}Nb(g.s., $9/2^+$)	^{94}Mo(0.87 MeV, 2^+)	$+p$	$1g_{9/2}$	7.619	1.0	[a]	
^{12}C(g.s., 0^+)	^{13}C(g.s., $1/2^-$)	$+n$	$1p_{1/2}$	4.496	0.274	0.26–0.43	[46]
						0.58	[47]
^{12}C(g.s., 0^+)	^{13}C(3.68 MeV, $3/2^-$)	$+n$	$1p_{3/2}$	1.262	1.750	0.36	[47]
^{93}Nb(g.s., $9/2^+$)	^{92}Nb(g.s., 7^+)	$-n$	$2d_{5/2}$	8.830	0.36	0.36	
^{93}Nb(g.s., $9/2^+$)	^{92}Nb(0.136 MeV, 7^+)	$-n$	$2d_{5/2}$	8.966	0.20	0.20	
^{93}Nb(g.s., $9/2^+$)	^{92}Nb(0.226 MeV, 2^-)	$-n$	$1f_{5/2}$	9.056	0.163	[b]	
^{93}Nb(g.s., $9/2^+$)	^{92}Nb(0.286 MeV, 3^+)	$-n$	$2d_{5/2}$	9.116	0.13	0.13	[48]
^{93}Nb(g.s., $9/2^+$)	^{92}Nb(0.357 MeV, 5^+)	$-n$	$2d_{5/2}$	9.187	0.10	0.10	
^{93}Nb(g.s., $9/2^+$)	^{92}Nb(0.390 MeV, 3^-)	$-n$	$2p_{3/2}$	9.220	0.137	[b]	
^{93}Nb(g.s., $9/2^+$)	^{92}Nb(0.480 MeV, 4^+)	$-n$	$2d_{5/2}$	9.310	0.180	0.180	
^{93}Nb(g.s., $9/2^+$)	^{92}Nb(0.501 MeV, 3^-)	$-n$	$2d_{5/2}$	9.331	0.180	0.180	
^{12}C(g.s., 0^+)	^{13}N(g.s., $1/2^-$)	$+p$	$1p_{1/2}$	1.943	0.53	0.53	[47]
^{12}C(g.s., 0^+)	^{13}N(2.365 MeV, $1/2^+$)	$+p$	$2s_{1/2}$	0.423	1.0	1.0	[49]
^{93}Nb(g.s., $9/2^+$)	^{92}Zr(g.s., 0^+)	$-p$	$1g_{9/2}$	6.043	0.36	[a]	
^{13}C(g.s., 0^+)	^{14}C(g.s., 0^+)	$+n$	$1p_{3/2}$	8.177	1	1.63	[50]
^{13}C(g.s., 0^+)	^{14}C(6.589 MeV, 0^+)	$+n$	$1p_{1/2}$	1.588	1	[a]	
^{13}C(3.68 MeV, $3/2^-$)	^{14}C(g.s., 0^+)	$+n$	$1p_{3/2}$	11.857	1	[a]	
^{13}C(3.68 MeV, $3/2^-$)	^{14}C(6.589 MeV, 0^+)	$+n$	$1p_{3/2}$	5.268	1	[a]	
^{92}Nb(g.s., 7^+)	^{91}Nb(g.s., $9/2^+$)	$-n$	$1g_{9/2}$	7.887	1	[a]	

[a] S values extracted in the present work.
[b] S values obtained by averaging the S values for nearby energy states.

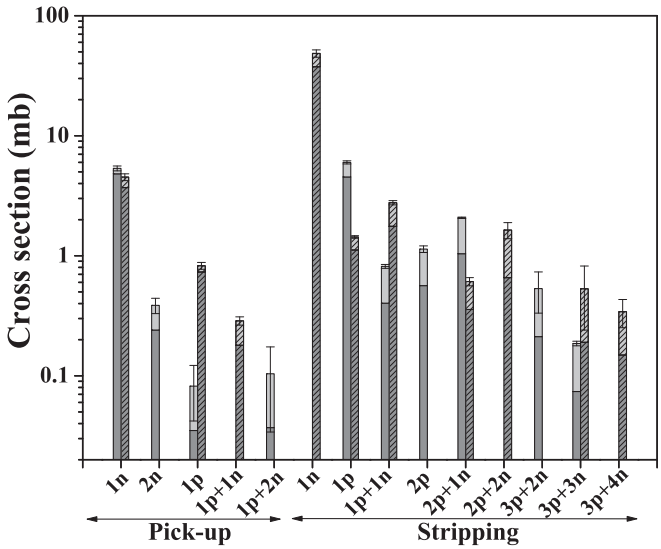

FIG. 9. Experimental cross sections of PLFs formed in different transfer (stripping and pick-up) reactions. Filled bars represent the cross sections of the PLFs formed in the $^{12}C + ^{93}Nb$ system and bars with slanting lines represent the same but for the $^{13}C + ^{93}Nb$ system. Dark-gray parts of the bars represent the cross section corresponding to the angular range covered in the experiment, and light-gray parts of the bars represents the cross sections obtained by extrapolation of the fitting up to 0° and 180°.

"$1p + 1n$" pick-up channel in $^{12}C + ^{93}Nb$ system could not be obtained as angular distribution for this channel a flat nature with large uncertainties. Also, the formation cross section for the "$2p + 2n$" stripping channel could not be obtained due to the break-up of the corresponding PLF ^{8}Be into two alpha particles. The Q_{gg} values for different stripping and pick-up reactions are shown in Fig. 10 to

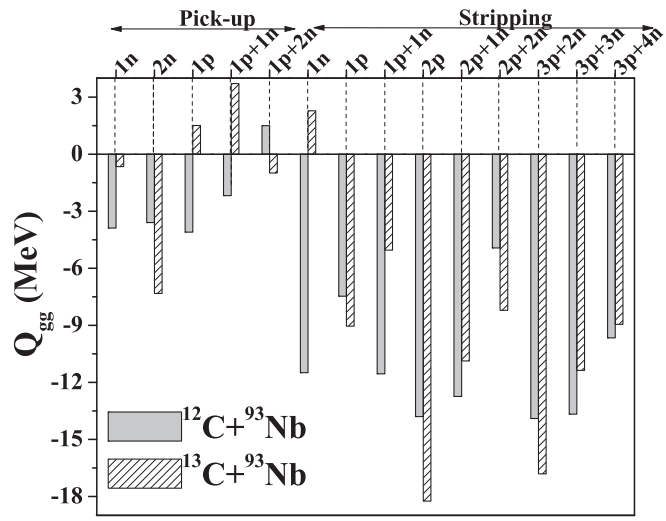

FIG. 10. Q_{gg} values for different reaction channels in $^{12,13}C + ^{93}Nb$. Filled bars are for $^{12}C + ^{93}Nb$ system and bars with slanting lines are for $^{13}C + ^{93}Nb$ system.

investigate the correlation between the yields of the PLFs and the corresponding Q_{gg} values. It can be seen from Fig. 10 that the Q_{gg} value for one-neutron pick-up in the $^{13}C + ^{93}Nb$ reaction is less negative than that in the $^{12}C + ^{93}Nb$ reaction. However, the observed yield for ^{14}C formed in one-neutron pick-up in the $^{13}C + ^{93}Nb$ reaction is lower than the yield of ^{13}C formed in one-neutron pick-up in the $^{12}C + ^{93}Nb$ reaction. This observation suggests that the higher N/Z ratio of the ^{13}C projectile may not favor pick-up of one more neutron to form ^{14}C. Absence of the "$2n$" and "$1p + 2n$" pick-up channels in the $^{13}C + ^{93}Nb$ reaction, corresponding to the formation of TLFs with $N = 50$, may also be due to the higher N/Z ratio of the ^{13}C projectile than that of ^{12}C. This observation suggests that the projectile N/Z ratio is also important to observe the effect of target structure in transfer reactions. Observation of large cross sections for the one-neutron stripping channel in the $^{13}C + ^{93}Nb$ reaction can be attributed to the presence of an unpaired neutron in ^{13}C which, after stripping, forms the more stable ^{12}C with $Q_{gg} = 2.281$ MeV. This channel was difficult to observe in the $^{12}C + ^{93}Nb$ reaction due to large background contributions of elastically scattered beam particles, suggesting a very low cross section for ^{11}C, even if it is formed. Similarly, the higher yield of the "$1p + 1n$" stripping channel in $^{13}C + ^{93}Nb$ as compared with $^{12}C + ^{93}Nb$ can also be due to the presence of the unpaired neutron in ^{13}C. Observation of significantly lower yield of the one-proton stripping channel in $^{13}C + ^{93}Nb$ as compared with $^{12}C + ^{93}Nb$ is possibly due to the higher N/Z ratio of ^{12}B (formed with the ^{13}C projectile with $Q_{gg} = -9.043$ MeV) as compared with the N/Z ratio of ^{11}B (formed with the ^{12}C projectile with $Q_{gg} = -7.47$ MeV). The formation cross sections of the PLFs associated with larger mass transfer between projectile and target may not be reasonably correlated with the Q_{gg} value because their formation would involve a dominant contribution from the more dissipative deep inelastic type of reaction mechanism.

IV. CONCLUSIONS

Kinetic-energy spectra and angular distributions of the projectile-like fragments have been measured for $^{12,13}C + ^{93}Nb$ reactions. The results show that, in the $^{12}C + ^{93}Nb$ reaction, there is an enhancement in the yield of ^{15}N formed along with ^{90}Zr having the closed-shell configuration with 50 neutrons and 40 protons, suggesting the role of the target structure on transfer reactions. A significant cross section was also observed for the two-neutron pick-up channel in the case of the $^{12}C + ^{93}Nb$ reaction, further highlighting the role of $N = 50$ shell closure. However, these channels were not detected in the case of the $^{13}C + ^{93}Nb$ reaction, demonstrating the importance of projectile structure for observing the effect of target structure in transfer reactions. Several states of the projectile- and the target-like fragments involved in the stripping and pick-up reactions were identified. One-neutron pick-up was observed to involve less energy transfer than one-proton stripping, which predominantly populated excited states. Also, in the kinetic-energy spectra for the proton-stripping channel, significant tailing was observed in the lower-energy side for both $^{12,13}C + ^{93}Nb$ reactions indicating substantial kinetic-energy dissipation. The angular distributions of PLFs for both reaction systems showed a systematic increase in forward peaking with decreasing mass. This observation indicates substantial interpenetration of the projectile and the target nuclei in the formation of lighter PLFs. Coupled reaction channels calculations have been performed using the code FRESCO to describe the angular distributions for inelastic scattering and of PLFs involving population of specific states of PLFs and TLFs in $^{12,13}C + ^{93}Nb$ reactions. Spectroscopic factors from the literature were used in the calculations wherever available, although they were modified in a few cases to match the experimental peak cross sections. Those channels, for which the spectroscopic factors were not available, have been assigned new spectroscopic factors in the present work. Calculated angular distributions were in reasonable agreement with the experimental angular distributions. However, it was observed that experimental angular distributions were more forward peaked; the deviation being more pronounced for the excited states. The maximum deviation was observed for the angular distribution of ^{14}C (6.589 MeV, 0^+ excited state) formed in the two-neutron pick-up channel in the $^{12}C + ^{93}Nb$ reaction. A systematic comparison of the cross sections of PLFs in ^{12}C- and ^{13}C-induced reactions shows the importance of projectile structure as well as the reaction Q_{gg} value in governing the transfer contributions.

[1] P. Misaelides, Radiochim. Acta **28**, 1 (1981).

[2] M. S. Zisman, F. D. Becchetti, B. G. Harvey, D. G. Kovar, J. Mahoney, and J. D. Shermant, Phys. Rev. C **8**, 1866 (1973).

[3] B. S. Tomar, A. Goswami, A. V. R. Reddy, S. K. Das, P. P. Burte, S. B. Manohar, and S. Prakash, Z. Phys. A: Hadrons Nucl. **343**, 223 (1992).

[4] E. Z. Buthelezi, F. Cerutti, E. Gadioli, G. F. Steyn, A. Pepe, S. H. Connell, and A. A. Cowley, Eur. Phys. J. A **28**, 193 (2006).

[5] A. Yadav, V. R. Sharma, P. P. Singh, D. P. Singh, R. Kumar, Unnati, M. K. Sharma, B. P. Singh, R. Prasad, and R. K. Bhowmik, Phys. Rev. C **85**, 064617 (2012).

[6] R. Tripathi, K. Sudarshan, S. Sodaye, and A. Goswami, J. Phys. G: Nucl. Phys. **35**, 025101 (2008).

[7] R. Tripathi, K. Sudarshan, S. Sodaye, A.V. R. Reddy, A. Goswami, B. K. Nayak, and S. K. Sharma, Phys. Rev. C **79**, 064604 (2009).

[8] R. Ali, D. Singh, M. A. Ansari, M. H. Rashid, R. Guin, and S. K. Das, J. Phys. G **37**, 115101 (2010).

[9] D. Singh, R. Ali, M. A. Ansari, B. S. Tomar, and M. H. Rashid, Nucl. Phys. A **879**, 107 (2012).

[10] V. V. Parkar, S. K. Sharma, R. Palit, S. Upadhyaya, A. Shrivastava, S. K. Pandit, K. Mahata, V. Jha, S. Santra, K. Ramachandran, T. N. Nag, P. K. Rath, B. Kanagalekar, and T. Trivedi, Phys. Rev. C **97**, 014607 (2018).

[11] D. Chattopadhyay, S. Santra, A. Pal, A. Kundu, K. Ramachandran, R. Tripathi, B. J. Roy, T. N. Nag, Y. Sawant,

B. K. Nayak, A. Saxena, and S. Kailas, Phys. Rev. C **97**, 051601(R) (2018).
[12] S. Sodaye, K. Sudarshan, B.S. Tomar, A. Goswami, S. Mukherjee, and K. Mahata, Eur. Phys. J. A **14**, 371 (2002).
[13] M. K. Sharma, Unnati, B. K. Sharma, B. P. Singh, H. D. Bhardwaj, R. Kumar, K. S. Golda, and R. Prasad, Phys. Rev. C **70**, 044606 (2004).
[14] C. Gerschel, Nucl. Phys. A **387**, 297 (1982).
[15] K. Sudarshan, S. Sodaye, K. Surendra Babu, S. Mukherjee, S. K. Rathi, K. Mahata, A Goswami, and B. S. Tomar, Phys. Rev. C **69**, 027603 (2004).
[16] A. D. Torres, J. Phys. G: Nucl. Phys. **37**, 075109 (2010).
[17] H. Morgenstern, W. Bohne, W. Galster, and K. Grabisch, Z. Phys. A **324**, 443 (1986).
[18] S. Sodaye, B. S. Tomar, and A. Goswami, Pramana **66**, 985 (2006).
[19] D. Singh, R. Ali, M. Afzal Ansari, B. S. Tomar, M. H. Rashid, R. Guin, and S. K. Das, Phys. Rev. C **83**, 054604 (2011).
[20] K. S. Babu, R. Tripathi, K. Sudarshan, S. Sodaye, A. Goswami, B. D. Shrivastava, and B. S. Tomar, Nucl. Phys. A **739**, 229 (2004).
[21] R. Tripathi, K. Sudarshan, S. Sodaye, S. K. Sharma, A. V. R. Reddy, and A. Goswami, Eur. Phys. J. A **42**, 25 (2009).
[22] B. S. Tomar, A. Goswami, G. K. Gubbi, A. V. R. Reddy, S. B. Manohar, B. John, and S. K. Kataria, Phys. Rev. C **58**, 3478 (1998).
[23] A. Kumar, R. Tripathi, S. Sodaye, K. Sudarshan, and P. K. Pujari, Eur. Phys. J. A **49**, 3 (2013).
[24] K. S. Babu, R. Tripathi, K. Sudarshan, B. D. Shrivastava, A. Goswami, and B. S. Tomar, J. Phys. G: Nucl. Phys. **29**, 1011 (2003).
[25] B. S. Tomar, A. Goswami, A. V. R. Reddy, S. K. Das, P. P. Burte, S. B. Manohar, and B. John, Phys. Rev. C **49**, 941 (1994).
[26] S. K. Pandit, A. Shrivastava, K. Mahata, V. V. Parkar, R. Palit, N. Keeley, P. C. Rout, A. Kumar, K. Ramachandran, S. Bhattacharyya, V. Nanal, C. S. Palshetkar, T. N. Nag, S. Gupta, S. Biswas, S. Saha, J. Sethi, P. Singh, A. Chatterjee, and S. Kailas, Phys. Rev. C **96**, 044616 (2017).
[27] T. Udagawa and T. Tamura, Phys. Rev. Lett. **45**, 1311 (1980).
[28] V. I. Zagrabaev, Ann. Phys. **197**, 33 (1990).
[29] B. G. Harvey, Nucl. Phys. A **444**, 498 (1985).
[30] M. H. Simbel and A. Y. Abul-Magd, Z. Phys. A **294**, 277 (1980).
[31] M. Stern, E. Gerlic, R. Billerey, B. Chambon, A. Chevarier, N. Chevarier, B. Cheynis, D. Drain, C. Pastor, and C. V. Donnet, Nucl. Phys. A **559**, 401 (1993).
[32] J. Wilczynski, K. Siwek-Wilczynska, J. Van Driel, S. Gonggrijp, D. C. J. M. Hageman, R. V. F. Janssens, J. Lukasiak, R. H. Siemssen, and S. Y. Van Der Werf, Nucl. Phys. A **373**, 109 (1982).
[33] I. J. Thompson, *Nuclear Theory and Modelling* (Livermore National Laboratory, Livermore, CA) 94551, USA and Department of Physics, University of Surrey, Guildford GU2 7XH, England, Version FRES 2.9, September 2011, LLNL-SM-485670.
[34] A. Chatterjee, A. Navin, A. Shrivastava, S. Bhattacharyya, M. Rejmund, N. Keeley, V. Nanal, J. Nyberg, R. G. Pillay, K. Ramachandran, I. Stefan, D. Bazin, D. Beaumel, Y. Blumenfeld, G. de France, D. Gupta, M. Labiche, A. Lemasson, R. Lemmon, R. Raabe, J. A. Scarpaci, C. Simenel, and C. Timis, Phys. Rev. Lett. **101**, 032701 (2008).
[35] L. Acosta, A. M. Sánchez-Benítez, M. E. Gómez, I. Martel, F. Pérez-Bernal, F. Pizarro, J. Rodríguez-Quintero, K. Rusek, M. A. G. Alvarez, M. V. Andres, J. M. Espino, J. P. Fernández-García, J. Gómez-Camacho, A. M. Moro, C. Angulo, J. Cabrera, E. Casarejos, P. Demaret, M. J. G. Borge, D. Escrig *et al.*, Phys. Rev. C **84**, 044604 (2011).
[36] Yu. Ts. Oganessian, V. I. Zagrebaev, and J. S. Vaagen, Phys. Rev. Lett. **82**, 4996 (1999).
[37] P. K. Sahu, R. K. Choudhury, D. C. Biswas, and B. K. Nayak, Phys. Rev. C **64**, 014609 (2001).
[38] D. C. Biswas, P. Roy, Y. K. Gupta, B. N. Joshi, B. K. Nayak, L. S. Danu, B. V. John, R. P. Vind, N. Deshmukh, S. Mukherjee, A. K. Jain, and R. K. Choudhury, J. Phys. Conf. **381**, 012091 (2012).
[39] P. K. Sahu, A. Saxena, R. K. Choudhury, B. K. Nayak, D. C. Biswas, L. M. Pant, R. G. Thomas, and Y. S. Sawant, Phys. Rev. C **68**, 054612 (2003).
[40] S. K. Pandit, A. Shrivastava, K. Mahata, V. V. Parkar, N. Keeley, P. C. Rout, K. Ramachandran, C. S. Palshetkar, I. Martel, A. Kumar, A. Chatterjee, and S. Kailas, Phys. Rev. C **100**, 014618 (2019).
[41] S. K. Pandit, A. Shrivastava, K. Mahata, N. Keeley, V. V. Parkar, P. C. Rout, K. Ramachandran, I. Martel, C. S. Palshetkar, A. Kumar, A. Chatterjee, and S. Kailas, Phys. Rev. C **93**, 061602(R) (2016).
[42] F. S. Goulding and B. G. Harvey, Ann. Rev. Nucl. Sci. **25**, 167 (1975).
[43] M. C. Mermaz, R. Dayaras, J. Barrette, B. Berthier, D. M. DE Castro Rizzo, O. Cisse, R. Legrain, A. Pagano, and E. Pollacco, Nucl. Phys. A **441**, 129 (1985).
[44] J. B. Ball, Kinematics II: A nonrelativistic kinematics FORTRAN program to aid analysis of nuclear reaction angular distribution data, Report No. ORNL-3251, United States (1962), doi:10.2172/4799284.
[45] E. T. Li, Z. H. Li, Y. J. Li, B. Guo, Y. B. Wang, D. Y. Pang, J. Su, S. Q. Yan, S. Zeng, L. Gan, Z. C. Li, J. C. Liu, X. X. Bai, Z. D. Wu, S. J. Jin, L. Y. Zhang, X. Q. Yu, L. Li, H. B. Sun, G. Lian, Q. W. Fan, and W. P. Liu, Phys. Rev. C **90**, 067601 (2014).
[46] X. D. Liu, M. A. Famiano, W. G. Lynch, M. B. Tsang, and J. A. Tostevin, Phys. Rev. C **69**, 064313 (2004).
[47] C. A. Pearson, J. M. Covan, and D. Zissermann, Nucl. Phys. A **191**, 1 (1972).
[48] M. A. Rumore, S. A. Dickey, C. A. Fields, and J. J. Kraushaar, Nucl. Phys. A **423**, 350 (1984).
[49] C. D. Nesaraja, C. R. Brune, B. T. Crowley, J. H. Kelley, S. O. Nelson, R. M. Prior, K. Sabourov, D. R. Tilley, A. Tonchev, and H. R. Weller, Phys. Rev. C **64**, 065804 (2001).
[50] M. B. Tsang, J. Lee, and W. G. Lynch, Phys. Rev. Lett. **95**, 222501 (2005).